Todo list

Simulation and characterization of integrated optics beam combiners for astrointerferometry

I. Physikalisches Institut
Universität zu Köln

Author :
Thomas Poletti
M1 Physics and NanoSciences
School-year 2017-2018

Supervisor:
Pr. Dr. Lucas Labadie
labadie@ph1.uni-koeln.de

Abstract

abstract-text

Résumé

Résumé ici

Contents

List of Figures

List of Tables

Introduction

Since antiquity and down to our time, astronomers always tried to see further and further in space requiring more and more sensitive instruments. Increasing the telescope diameter is one way to reach higher angular resolution but in the same time make it more sensitive to atmospheric turbulence. Therefore even with the recent progress in adaptative optics, today's largest telescopes can only can only resolve few of the brightest and nearest stars.

Using individual telescopes to form an interferometer, the resolution is determined by the distance between the telescopes. Until recently the instruments combining the light from individual telescopes were bases on costly and cumbersome bulk optics. The recent advances in manufacturing integrated-optics and especially in laser processing have resulted in new instruments that are operational on sky and delivering higher quality results.

The purpose of this work is to optimise and characterise the performance of Integrated optic (IO) beam combiners and especially one promising type of component called discrete beam combiner (DBC). Allowing to retrieve the astronomical parameters without scanning the interferogram these components could allow to observe fast varying objects.

This report is organised in three parts. In the first part I will present the motivation and the basis of astronomical interferometry. In the second part will be presented the simulation results of the DBC as well as its optimisation. In the last part will be discussed the experimental characterisation of asymmetric couplers, Multi Mode Interferometer (MMI) and of the DBC.

1 Motivation and scientific background

- quoi quest-ce linterferometrie, intérêt par rapport à lobservation par un télescope mono-pupille en terme de résolution angulaire - nulling, contraintes - schema hi-5, explications - VLTI - bandes dobservation - unités astro - Bases de la BeamPropMethod

2 Simulation of the DBC

The discrete beam combiner is a component made of multiple straight waveguides close to each other. It has been demonstrated that in the case of a N telescope DBC, an array of more than N^2 waveguides is needed for efficient operation of the DBC [Min12]. But at this point is hasn't been studied the impact of other geometrical parameters such as the spacing between each waveguides.

The component studied is formed of 23 outputs and four inputs to combine the light from four individual telescopes. A cross-section of it is shown on Fig. 1. Both the input configuration and the "Zig-Zag" shape have already been optimised. After a brief explanation of the theory behind the DBC we will focus on optimising it regarding P_x,

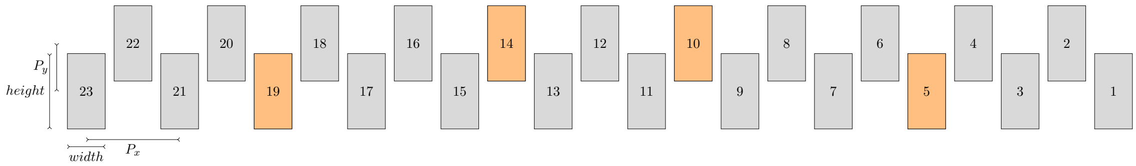

Figure 1: The Zig-Zag array's cross section with the numbering convention. The four input waveguides are displayed in orange.

P_y, *width*, *height* and the length of the DBC part (the notations refers to Fig. 1) in the case of monochromatic light. In a second part the performances of the optimised component regarding the bandwidth of the input light are simulated. All simulation are performed using the commercial software Beamprop in scalar mode (a full-vectorial mode would have been more accurate but didn't show much different results for both TE and TM polarisation regarding the condition number of the Visibility to Pixel Matrix (V2PM) -see next section-), correlation mode and transparent boundary condition. The grid size was chosen as a balance between computation time and accuracy.

2.1 Monochromatic light

In this section is shown the impact on the performances of the DBC regarding its geometry. Two main parameters are studied, the condition number of the V2PM and the throughput as it hadn't been done before.

2.1.1 Mathematical formalism

As stated before the "Zig-Zag" DBC is composed of 23 outputs and can combine the light from 4 individual telescopes. This component has the particularity that all the information about the coherence function of the studied object is included in the way the 23 outputs are related to each other [TMC$^+$07]. In the case of monochromatic light the theory is exact. We will do a brief overview of the theoretical background in this part. For further reading the reader can refer to [TMC$^+$07, SMD$^+$13, DTL$^+$17].

In this part we will consider the light combined from the input A and B at the n^{th} output. In that case the intensity I_n at the output can be expresed as :

$$I_n = \kappa_A I_A + \kappa_B I_B + 2\sqrt{\kappa_A I_A \kappa_B I_B} V_{AB}^{inst} V_{AB}^{obj} \cos(\phi_{AB}^{inst} + \phi_{AB}^{obj}) \tag{1}$$

In this equation κ_i is the transmission coefficient from the input i to the considered output. *inst* and *obj* relates the visibility/phases of the instrument and of the observed object. Equation 1 can easily be reduced to Eq.2 in which the produce of the instrumental and object visibility are reduced in V_{AB}.

$$I_n = \kappa_A I_A + \kappa_B I_B + 2\sqrt{\kappa_A I_A \kappa_B I_B} V_{AB} \left(\cos(\phi_{AB}^{inst}) \cos(\phi_{AB}^{obj}) - \sin(\phi_{AB}^{inst}) \sin(\phi_{AB}^{obj}) \right) \tag{2}$$

From Eq.2 the problem of getting the object mutual coherence function can be reduced to the produce of a matrix and a vector. Thus the characteristics of the input fields can be linked to the output intensities by the relation :

$$\vec{I} = V2PM \times \vec{V} \tag{3}$$

In which $\vec{I} = (I_1, ...I_M)^T$ represent the intensities at the M outputs,
$\vec{V} = (I_1, ..., I_M, V_{12}^{obj}\sqrt{I_1 I_2} cos(\Phi_{21}^{obj}), V_{12}^{obj}\sqrt{I_1 I_2} sin(\Phi_{21}^{obj}), ..., V_{N-1,N}^{obj}\sqrt{I_{N-1} I_N} cos(\Phi_{N,(N-1)}^{obj}), V_{N-1,N}^{obj}\sqrt{I_{N-1} I_N} sin(\Phi_{N,(N-1)}^{obj}))$
and the visibility to pixel matrix V2PM represent the beam combiner's properties. An example of a V2PM for an hypothetical beam combiner with 3 inputs and 2 outputs is displayed in Figure 2

$$\begin{pmatrix} \kappa_{11} & \kappa_{21} & \kappa_{31} & 2V_{12}^1\sqrt{\kappa_{11}\kappa_{21}} cos(\Phi_{12}^{inst}) & -2V_{12}^1\sqrt{\kappa_{11}\kappa_{21}} sin(\Phi_{12}^{inst}) & 2V_{13}^1\sqrt{\kappa_{11}\kappa_{31}} cos(\Phi_{13}^{inst}) & -2V_{13}^1\sqrt{\kappa_{11}\kappa_{31}} sin(\Phi_{13}^{inst}) & 2V_{23}^1\sqrt{\kappa_{21}\kappa_{31}} cos(\Phi_{23}^{inst}) & -2V_{23}^1\sqrt{\kappa_{21}\kappa_{31}} sin(\Phi_{23}^{inst}) \\ \kappa_{12} & \kappa_{22} & \kappa_{32} & 2V_{12}^2\sqrt{\kappa_{12}\kappa_{22}} cos(\Phi_{12}^{inst}) & -2V_{12}^2\sqrt{\kappa_{12}\kappa_{22}} sin(\Phi_{12}^{inst}) & 2V_{13}^2\sqrt{\kappa_{12}\kappa_{32}} cos(\Phi_{13}^{inst}) & -2V_{13}^2\sqrt{\kappa_{12}\kappa_{32}} sin(\Phi_{13}^{inst}) & 2V_{23}^2\sqrt{\kappa_{22}\kappa_{32}} cos(\Phi_{23}^{inst}) & -2V_{23}^2\sqrt{\kappa_{22}\kappa_{32}} sin(\Phi_{23}^{inst}) \end{pmatrix}$$

Figure 2: An hypothetical V2PM matrix for a 3 to 2 beam combiner. All visibility and phases in the matrix are the instrumental ones.

One can find the Pixel to Visibility Matrix (P2VM) by inverting the V2PM matrix with the relation 4 and then the astronomical information from $\vec{V}$. To be consistent with the notation introduced in [SMD+13], $\vec{V} = (\Gamma_{11}, ..., \Gamma_{MM}, \mathcal{R}\Gamma_{12}, \mathcal{I}\Gamma_{12}, ..., \mathcal{R}\Gamma_{N(N-1)}, \mathcal{I}\Gamma_{N(N-1)})$ the object phase and visibility can be extracted by :

$$V_{ij}^{obj} = \sqrt{\frac{(\mathcal{R}\Gamma_{ij})^2 + (\mathcal{I}\Gamma_{ij})^2}{\Gamma_{ii}\Gamma_{jj}}} \qquad \Phi_{ij}^{obj} = arctan(\frac{\mathcal{I}\Gamma_{ij}}{\mathcal{R}\Gamma_{ij}}) \quad i \neq j$$

$$P2VM = (V2PM^T \times V2PM)^{-1} \times V2PM^T \tag{4}$$

In the light of this formalism the retrieved coherence function from the P2VM can be inaccurate and one has to minimize the condition number of the matrix in order to minimize the possibility of a strong amplification of measure inaccuracy. For further explanation on this subject refers to Annexe A.1.

To characterise the instrumental phase and visibility at an output a coherent source is used (thus the object's visibility is 1 and the phase visibility is 0). A cosine is fitted to the simulated curve of the intensity at an output. Than photocorrection5 is then applied using the intensity simulated with only one input beam used. This process is repeated for all 6 baselines to build all the V2PM.

$$V_n(x) = \frac{I_n(x) - \kappa_A I_A - \kappa_B I_B}{2\sqrt{\kappa_A I_A \kappa_B I_B}} = V_{AB}^{inst} V_{AB}^{obj} \cos(\phi_{AB}^{inst} + \phi_{AB}^{obj}) \tag{5}$$

2.1.2 Impact of evanescent coupling on the output power

The main principle behind the the DBC being the coupling of electromagnetic fields, it is important to understand how much the area chosen to calculate the power at an output could affect the phases relations and visibility. This part focuses on this problem.

Considering only 3 distinct wave-guides of the DBC Zig-Zag component. The cross section of each WG is a rectangle $width \times height$. In such a dielectric wave-guide, there is no analytical solution to the scalar wave equation but according to [Lab08] a good approximation of the transverse field profile is close to a gaussian :

$$\Psi(x,y) \approx \Psi_0 exp\left(\frac{-x^2}{\omega_x^2} + \frac{-y^2}{\omega_y^2}\right)$$

Using this equation and retrieving ω_x and ω_y from BeamProp simulation by the width of the gaussian at $1/e$ of its maximal amplitude, we can «calculate» the transverse field profile in the wave-guide.

We simulate this behaviour for the following parameters (in µm) :

- Px =24
- Py = 10.8
- width = 9.5
- height = 17
- $n_{clad} = 2.31$
- $\delta n = 0.005$

In this case we have $\omega_x \approx 7.798$ and $\omega_y \approx 10.114$. The resulting field for 3 outputs in phase and guiding the same power is shown in Fig. 3.

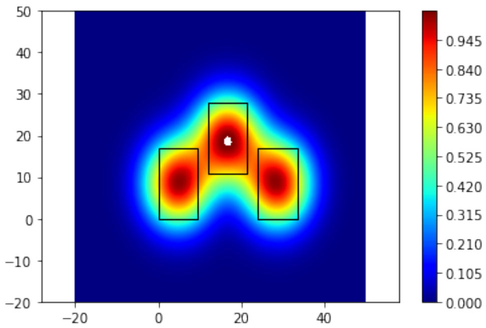

Figure 3: Example of 3 outputs in phase guiding the same power. The modes are Gaussian perfectly centred on the wave-guide

One can see that in this case, where the 3 outputs are in phase, the determination of the power in the middle WG will be badly estimated by a simple power integral as :

$$P \propto \iint_{\mathbb{R}^2} \Psi^*(x, y)\Psi_{sim}(x, y)dxdy \tag{6}$$

where Ψ_{sim} is the simulated output fields as shown on the upper figure. Actually the exact knowledge of the power guided through one individual output is not needed. But if the outputs are not in phase, estimating the "power" by the previous integral would lead to harmonic in the signal vs the optical path difference (OPD). Therefore the integration should be limited to a small area around the WG. In the next paragraph we verify the impact of this choice on the phases relations, instrumental visibility thus the V2PM.

Power of a Gaussian field : For an isolated gaussian field the power P is given by

$$\frac{P}{\Psi_0^2} \propto \iint_{\mathbb{R}^2} exp\left(\frac{-2x^2}{\omega_x^2} + \frac{-2y^2}{\omega_y^2}\right) dxdy = \frac{\pi}{2}\omega_x\omega_y$$

In the case of our parameters the right hand is equal to 123.88 µm^2 (a numerical integration using the composite trapezoidal rule lead to 123.76). By integrating the whole field as represented in Fig. 3 over the cross-section we obtain 113.70 µm^2 but the truly guided power in the central wave-guide calculated over the cross-section should only be 87.39 µm^2 thus an error of 30 %.
In the opposite case where there is no power in the central wave-guide, and a maximal power in the two surrounding wave-guides we find a guided power in the central wave-guide over the cross-section of 3.10 µm^2. It can easily be understood that the simulated (ergo the experimental) interferograms will depend of the considered area. The larger this area, the greater the impact of the surrounding wave-guides on the interferogram. In an other hand the smaller this area, the smaller the signal to noise ratio.

Influence on the simulated phases relations : We have seen that the integrating area used to estimate the guided power should have a great impact on the result, we now try to see its impact on the simulated phase relations. To do this the 3 gaussian are multiplied by a cosine to simulate a phase dependency. The left and right outputs are set with phases pi/3 and 2pi/3 respectively and the middle one with phase 0. The power is then integrated on different area centred on the waveguide (WG) cross-section.

One can see that in this case, the phase of the output signal is mostly unchanged by the integrating area, but this is only the case for area slightly larger to the WG's cross section. Therefore it might be expected that the phase relation between outputs with comparable power magnitude will stay the same for low variation of the integrating area. The only changed parameter might be the Visibility but one can not conclude as the mean value, ergo the photometries changes too.

To this point we have only seen the impact of the integrating area when all outputs are guiding the same maximal power. It is now studied the impact on a low guided power in the middle WG comparatively to the left and right ones. Same phases are introduced. The power in the left and right WG are the same and 4 times the power in the middle WG. The results to those simulations are shown in Fig. 4

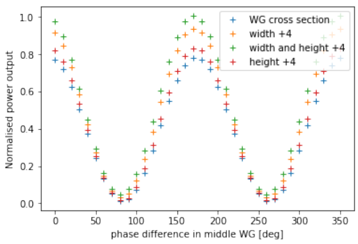

(a) Simulation with the same power in the middle and the surroundings WG.

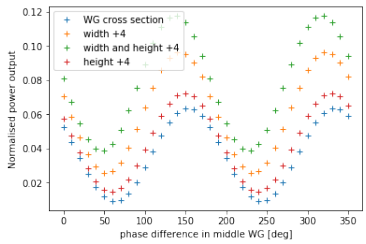

(b) Simulation with low power in the middle WG and high in the surroundings.

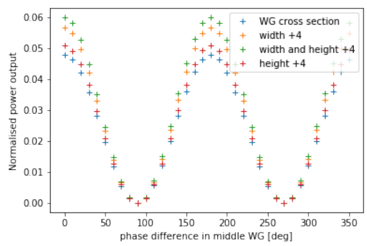

(c) Simulation with low power in the middle WG and high in the surroundings for a higher x spacing between the WG.

Figure 4: Influence of different parameters on the phases and amplitudes of the interferogram in the middle wave-guide. The phases relations between the outputs are highly influenced by the evanescent coupling

As can be seen, the more the power difference between the middle WG and the sides WG and the larger the integrating area, the more impacted the retrieved phase differences. Therefore it seems that the V2PM matrix of the component should be calculated not only for the isolated component but also with the imaging system. One way to get rid of these dependency would be to have a greater spacing between the WG at the output so that the evanescent coupling is as low as possible (as shown in Fig. 4c). Thus the use of a «fan out» could be an option to calculate the power over a larger area thus have a greater integrated power (ergo a smaller signal to noise ratio (SNR)).

2.1.3 Influence of geometrical parameters

Knowing the problem exposed in the previous section, the "ideal" surface over which the power is calculated has to be estimated. Then the influence of the geometrical parameters on the performances (estimated by the condition number of the V2PM) can be studied.

In all the following, the amplitude of visibility (or visibility) refers to V_{ij} (sometimes to the all function $V_{ij}cos(\phi_{ij})$ where ϕ_{ij} is a function of the OPD. A good approximation of ϕ_{ij} is $\frac{2\pi x}{\lambda}$ where x is the OPD. V and ϕ are both obtained by fitting the simulated curve with a cosine.

To estimate the critical surface, the power at an output versus the OPD is simulated using the software $BeamProp^{TM}$. It has been found that the presence of harmonics in the signal should not be higher than 2% of the main signal (the cosine). A surface corresponding to the waveguide's cross-section appeared to solve this problem for a wavelength of 3.8µm as shown on Fig.5b.

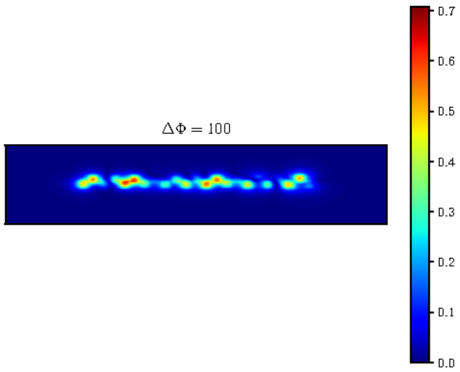

(a) Example of the output simulated field.

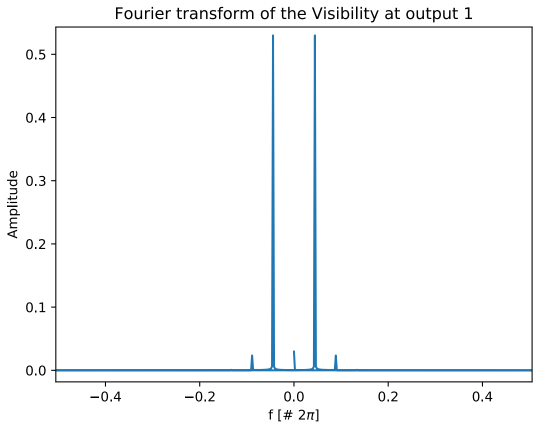

(b) Spectrum of the visibility at output 1

Figure 5: Origin and presence of harmonics in the output calculated power

All simulation unless explicitly written are performed using the previously determined integrating area. Moreover the base parameters : P_x = 24µm, P_y = 10.8µm, $width$ = 9.5µm, $height$ = 17µm, $\delta n = 0.005$, λ = 3.4µm, length of the DBC's part = 25mm, length of the input = 25mm, together with transparent boundary condition. The grid dimensions and z step are chosen as a balance between computation time and desired accuracy. For general results one can choose a «coarse» grid and then narrow it for more accurate results. Results presented are for scalar solution of the wave equation. Therefore they do not incorporate impacts of polarization effects. Moreover the material are supposedly perfects in the simulation (i.e. isotropic material, no absorption, no scattering...).

To ensure a good accuracy on the retrieved astronomical parameters, the V2PM's condition number must be as close to 1 as possible (see A.1). This part will be focused on lowering the V2PM's condition number by using different geometrical parameters. The launch fields are Gaussian of same power and of 1/e diameters the width and height of the wave-guide. Thus a coupling loss of approximately 10% occurs. Fresnel losses are not included.

X and Y spacing: Simulations were performed for different values of P_x and P_y to find which parameters minimizes the condition number. The results are shown in table 1. With the few tested parameters one can only conclude that the V2PM condition number seems to be minimum for $P_x \approx 24$µm and $P_y \approx 10.8$µm. Concerning the throughput, it seems to have a quite linear dependency with P_y and an exponential decay with P_x within the tested range (and only within the tested range as the throughput should stay between 0% and 100%). Fitted results are displayed in figure 6. Theses results are obtained for one set of parameters and should be valid only within the tested range.

Py $[\mu m]$ / **Px**$[\mu m]$	**4.8**	**6.8**	**8.8**	**10.8**	**12.8**
19				10.68 (67.1%)	
21				10.69 (63.1%)	
23				24.77 (61.5%)	
24	24.05 (62.3%)	32.6 (62.0%)	18.77 (61.7%)	7.16 (61.2%)	16.6 (60.8%)
25				11.7 (60.9%)	

Table 1: Condition number and throughput (in parenthesis) for several x and y spacing. The throughput is calculated by the sum of the power at each outputs normalized by the total input power. The power is calculated by a power integral of the simulated field over the wave-guide's cross-section

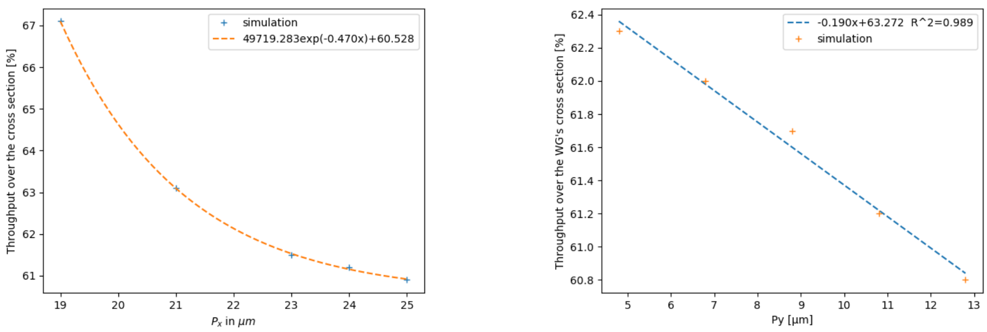

(a) (b)

Figure 6: Evolution of the throughput over the cross section with P_x and P_y at fixed cross-section and simulation parameters (see text for details). (a) at fixed $P_y = 10.8\mu m$, (b) at fixed $P_x = 24\mu m$

The cross section: Now that a minimum of the condition number regarding x and y spacing has been found, the wave-guide's dimensions has to be optimized too. In the tested range all dimensions ensure that the wave-guide is mono-mode to have all «ray» traveling at the same speed in z direction (in the fundamental mode, most of the energy is traveling close to the core of the WG). This is to ensure a low modal dispersion and low coupling losses of the input field. These simulations are performed for $P_x = 24$µm and $P_y = 10.8$µm.

height / width	**15**	**16**	**17**	18
7.5			5.07 (45.9%)	
8.5			8.00 (54.1%)	
9.5	7.76 (57.8%)	8.29 (59.5%)	7.16 (61.2%)	10.12 (62.4%)
10.5			14.6 (67.5%)	

Table 2: Condition number and throughput (in parenthesis) over the WG's cross-section for several width and height. The throughput is calculated by the sum of the power at each outputs normalized by the total input power. The power is calculated by a power integral of the simulated field over the wave-guide's cross-section

One more time a minimum of the condition number is found for $width = 7.5$µm and $height = 17$µm, but as such a width would lead to too much more refinance (which our simulation doesn't take into account) a width of 9.5µm will be used instead. The throughput seems to be linear for dimensions of the wave-guides slightly different. But only for dimensions closes to the simulated ones.

Optical index difference: The wave-guides used are rectangular dielectric wave-guides with step index. As a higher optical index difference lead to a stronger mode confinement, a higher throughput over the cross section is to be expected with a higher δn. This paragraph focuses on finding the best δn to have an higher throughput together with a low condition number of the V2PM matrix. In this simulation the previously «optimised» geometrical parameters are used (except for the width of the WGs which is $width = 9.5\mu m$) and the throughput is still calculated over the wave-guide cross-section. The results are shown in table 3.

It seems that the throughput evolves as the logarithm of δn within the tested range (and only within the tested range)(see fig.7).

The condition number seems to be minimum for $\delta_n = 0.004$ but as it is only of 1 lower than for $\delta_n = 0.005$ and the throughput over the wave-guide's cross-section is 10% greater in this case, $\delta_n = 0.005$ would be used as «optimised» optical index difference.

Lengths: An other parameter that has to be optimized is the length of the DBC's part. To this point all simulations were performed for a length of 25mm. An other length that

δn	condition number	throughput
0.002	61.3	23%
0.003	13.5	40%
0.004	6.1	52%
0.005	7.16	61%
0.006	15.0	68%
0.007	14.6	73%

Table 3: Condition number and throughput over the WG's cross-section for several values of δn. The throughput is calculated by the sum of the power at each outputs normalized by the total input power. The power is calculated by a power integral of the simulated field over the wave-guide's cross-section

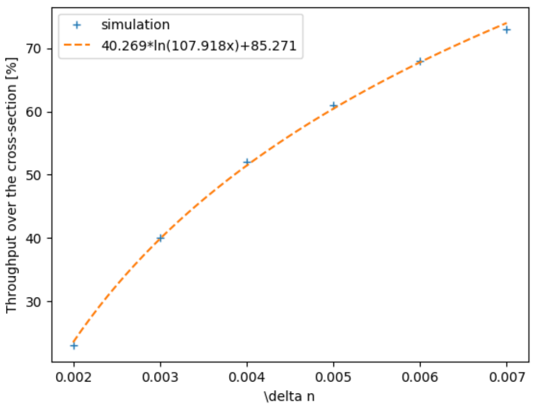

Figure 7: Throughput over the cross section for different optical index differences

could be optimized is the length of the inputs which were also to this point of 25mm, but as the x and y spacing of the inputs ensures that the fields aren't coupled, this shouldn't impact the V2PM condition number. This was verified in the simulation for length greater to $1cm$. The results are shown in figure 8. The «1/e» area refers to a rectangle of width and height the 1/e width and height of the fundamental mode of the wave-guide (for $\delta n = 0.005$ which should contains 91% of the mode power)

The simulations were performed for a length greater than 15mm to be sure that each inputs field propagates through the 23 outputs as can be seen in the figure 9a.

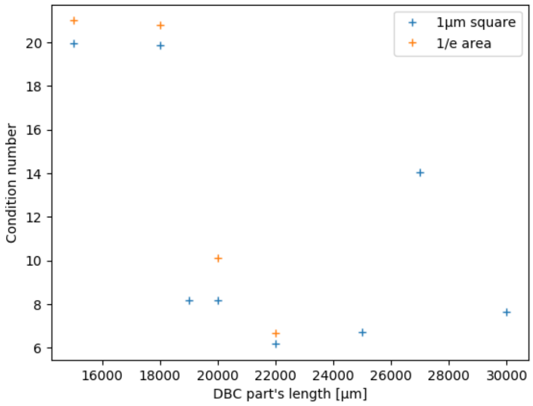

Figure 8: Condition number of the V2PM matrix for different lengths of the DBC part. The power is calculated either over a 1 by 1 micrometer area or the «1/e» area centered on the cross-section. (see text for details)

One can notice that the condition number tend to be higher for a short length of the DBC's part, and have a minimum of 6.15 for a DBC part of 22mm long. Moreover with a higher power integrating area, the condition number seems to behave the same for a large or a small integrating area so that a minimum of the condition number found with an integrating area should remain a minimum for another (if the area isn't too large and doesn't overlap surrounding fields).

Concerning the throughput, it seems to be constant within the tested length (see Fig.9b). Of course our simulated WG doesn't include scattering, surfaces defaults etc. The only kinds of losses that occurs in this simulation are bending losses and radiation in the cladding (absorption is negligible). The reader may have noticed a 10% higher throughput than in the previous sections. This is because the input field in this simulation is a Gaussian of «1/e» width and height the «1/e» width and height of the fundamental mode of the WG. Thus the 10% coupling losses experienced in the previous do not take place in this simulation.

It has be seen that the V2PM matrix is quite dependent of the area over which the power is calculated at the output. One possible way to minimise this dependency would be to

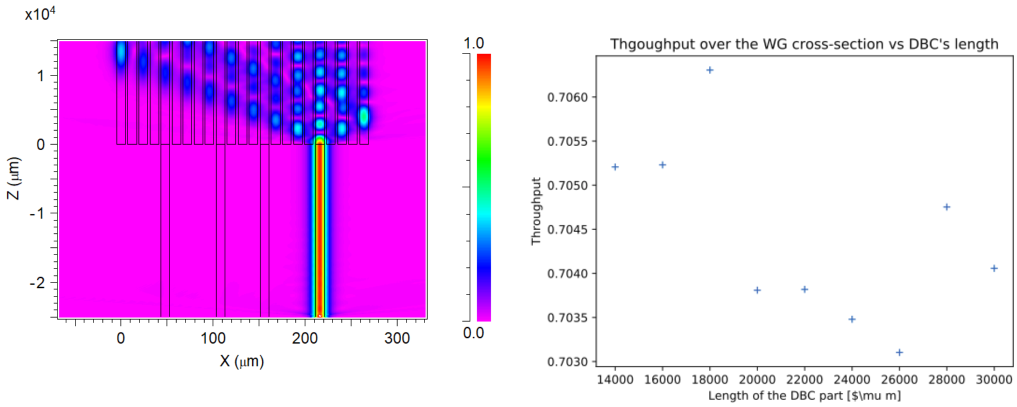

(a) Propagation of the scalar field from the 4th input. A length of 12mm seems to be a minimum to have the field reaching every single output.

(b) Throughput over the cross-section for different lengths of the DBC part. Two area are considered to estimate the power at the outputs (see text for details).

Figure 9

design a «fan-out». By increasing the spacing of the outputs, the field should be more centered and no overlapping would occur at the output. The next section will focus on this component.

2.1.4 Adding a «fan out»

We have seen that both the visibility and phases relations are dependent of the way the power is calculated. This is caused by the fields overlapping at the outputs. One way to get rid of this effect could be to add a «fan out» at the end of the DBC part and then be able to really take into account of all the flux when calculating the power. Simulations with this have been performed with a spacing of the outputs of 2 times the «$1/e^3$» width of the fundamental mode to be certain that no more overlapping will occur (see Fig. 10). By doing this one can estimate the power in a wave-guide over a finite area and knowing which percentage of the power of a Gaussian field is contained in the same area, retrieve the total guided power (assuming that the fundamental mode is a Gaussien). But the point is that with such a device, the way of calculating the power at the output should no more impact neither the visibility nor phases relations, ergo the V2PM condition number (as it is the case with the previous component for large integrating area). Therefore in these simulation the power is calculated by the power integral of the simulated field over the WG's cross-section. Results show that most of the visibility in that case are between 0.98 and 1.00 (without any polarization effects they should be all of 1) where they could be below 0.3 without the fan out. Moreover with the simulated design the fan-out lead to less than 3% losses (bending losses and radiation in the cladding) as the throughput over the WG's cross-section is up to 68%. A simulation of the throughput where the power at the end of each output is calculated over a large enough area to consider that all the power is being accounted we obtain 96.7% of throughput. This results could seems high but it is to be known that the simulations doesn't take into account scattering, material absorption (which might be very low for the considered material (GLS) at this wavelength) etc... Losses are only radiations in the cladding, bending losses and coupling losses with the input field (which we managed to get below 1% in this simulation). Moreover one can see that 68 is almost 71% of 96.7 which is the percentage of the true centered Gaussian field's power calculated over the cross-section of the WG. This shows that at the outputs the fields should be mostly Gaussian centered fields thus the «fan out» might be well designed.

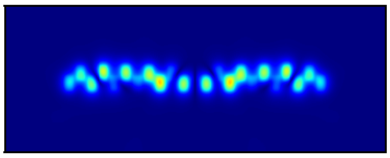

(a) Output of the ZigZag DBC without fan-out. Fields are highly overlapping and not centred in the WG.

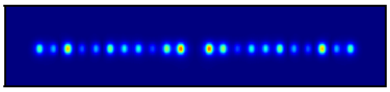

(b) Output of the ZigZag DBC with a «flat» fan-out. Fields are centered in the WG and not overlapping.

Figure 10: Effect of adding a «flat» fan-out at the output. The color-scale is the same (0 in blue to 0.6 in red) and the scalar field is displayed.

With this geometry of the «fan out», the condition number of the V2PM matrix seems to behave the same with the length of the DBC's part. The simulation leads to a condition number of 6.89 for a length of 22mm (11.61 for a length of 20mm and 7.87 for a length of 19mm). Table 4 show for 3 different length of the DBC part and for three area considered to calculate the power, how much the condition number is now «independent» of the considered area. It also seems that the component with the «fan out» behave the same

Area \ Length [mm]	18	20	22
$1/e^3$	7.77	11.73	6.89
Cross	7.87	11.61	6.90
$3\mu m$	7.92	11.64	6.89

Table 4: Condition number of the V2PM matrix for 3 different area used to calculate the power at the outputs. The «$1/e^3$» correspond to an area of 27×35µm (and contain more than 99% of the fundamental's power), the «Cross» is the wave-guide's cross section and the 3pixels to an area of 3×3µm

than the component without it except that the way the power is calculated at the output doesn't impact much more the V2PM matrix, visibility and phases relations as can be seen on figure 11. Of course the visibilities are still impacted but they still are greater than 95% for the majority (and greater than 0.75). In the case without the fan-out the visibilities were down to 0.4 or less.

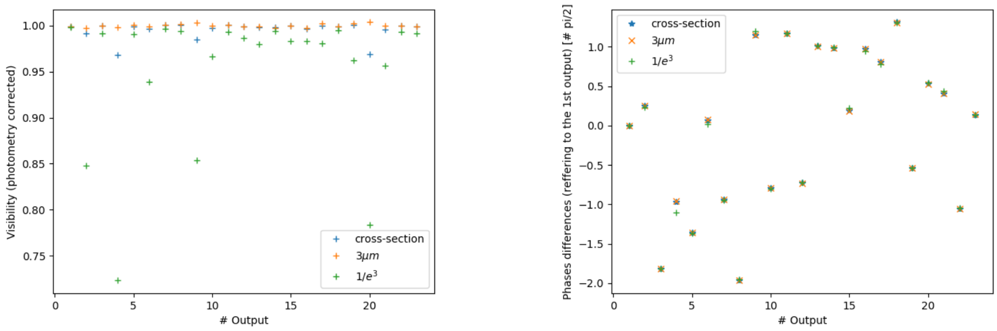

(a) (b)

Figure 11: Baseline 1-2 Visibilities (photometry corrected) and phases relations (referring to the first output) for 3 different area used to calculate the power at the outputs. The «$1/e^3$» correspond to an area of 27×35µm, the «1/e» to an area of 15.596×20.227µm and the 3pixels to an area of 3×3µm

Effect of polarization on the retrieved parameters To this point no polarization effects has been simulated. In this part the V2PM matrix is calculated using monochromatic TE and TM polarized light. It is then studied the impact of using a TM polarization calibrated V2PM on the TE polarization data to retrieve the astronomical parameters (and vice et versa).

First of all the V2PM calibrated matrix using TE polarized light show a condition number of 6.203 and it is 6.124 for the TM polarized light. In the case of the scalar field (no polarization effect) the condition number was 6.161 which is almost the mean of TE and TM ones. Those two V2PM matrices are used to retrieve the astronomical parameters from the simulated output fields. The results are shown in Tab.5 in which ϵ_i is calculated by $\epsilon_i = \sqrt{\sum \frac{1}{N}(a - \tilde{a})^2}$ where a is the data, $\tilde{a}$ the expected parameter (phase or visibility) and N the number of simulated phase and visibility. One can see that the error on the retrieved parameters are between 30 and 40 times higher when using the V2PM calibrated using polarized light on 90ř shifted polarized light. The impact is still very low and justify not taking into account the polarization for the previous simulation.

adaptability to other wavelength Before simulating the DBC using poly-chromatic light the dependence of the design regarding the wavelength is tested. Of course to have a component that behave the same at an other wavelength one can simply multiply its dimensions by the ratio of the wavelength. But as a component will have to be used

V2PM / data	TE		TM	
	ϵ_ϕ [rad]	ϵ_V[%]	ϵ_ϕ [rad]	ϵ_V[%]
TE	6.95×10^{-4}	7.14×10^{-4}	2.17×10^{-2}	2.51×10^{-2}
TM	2.08×10^{-2}	2.47×10^{-2}	6.36×10^{-4}	6.77×10^{-4}

Table 5: Error on the retrieved parameters from the V2PM calibrated using TE/TM polarized light. The TE/TM data refers as the simulated input fields.

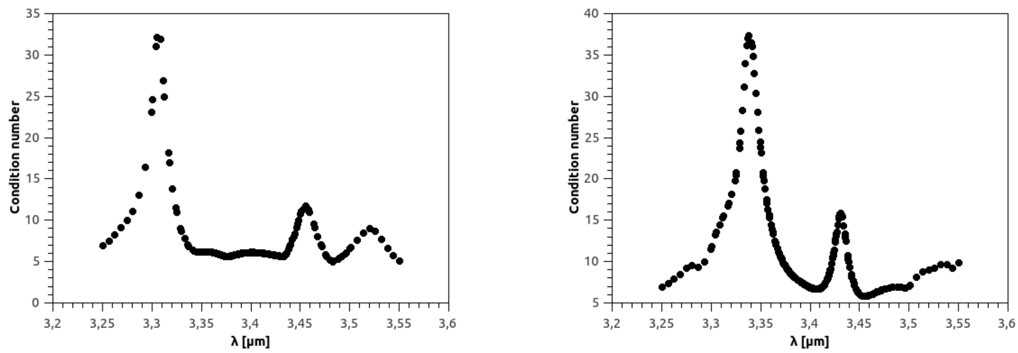

(a) (b)

Figure 12: Condition number of monochromatic V2PM matrices at different wavelength. (a) for the component without fan-out, (b) for the component with fan-out. The geometry of the component is the optimized one (see text for details)

using poly-chromatic light it is interesting to see how the condition number is influenced for a given design by the wavelength. The design previously "optimized" is used for this simulation. The results of this simulation are shown in Fig.12. As can be seen both of the curves are very similar in first sight. The component without fan-out show a flat curve for lambda ranging from 3.35 to 3.43 µm where for the component with fan-out this "flat zone" almost doesn't exist. This suggest that the component without fan-out could be more stable than the component with. This can be explained by the fact that the geometry of the fan-out act like if the coupling length were longer. This apparent length is strongly dependent of the wavelength because the coupling of the fields between two nearby waveguides are strongly dependents of the wavelength. The zone where the WGs separates will couple a larger wavelength for a longer length because of the larger overlap integral between the two individual WG's modes for higher wavelength. For further explanation on the coupled mode theory the reader can refers to [BEAS07, DM91].

The evolution of the V2PM's condition number regarding the geometrical parameters and the wavelength has been studied and an optimal configuration has been found. This configuration ensures a condition number of approximately 6 which means that an error on the measured output wouldn't be magnified more than 6 times (in the worst case) by the retrieving algorithm. The evolution of the "usable" throughput through a defined surface has also been studied and result of more than 96% in the case of the component with fan-out and 70% without. This throughput doesn't include the losses from coupling nor Fresnel which should be predominant for this component. The optimized parameters are given in Tab.6. All the previous work has been done using only monochromatic light. But the light from a star is obviously not monochromatic, an it's not wanted to use too narrow-band filters in order to keep high signal to noise ratio (SNR). This is the purpose of the next section.

P_x	2.4×10^1
P_y	1.08×10^1
$width$	9.5
$height$	1.7×10^1
δ	5×10^{-3}
λ	3.4
L_c	2.2000×10^4
L_i	1.0000×10^4
background index	2.31

Table 6: Optimised set of parameters (distance unit in µm)

2.2 Polychromatic light

In order to keep a high enough SNR and also for different needing, the component will be used under poly-chromatic light. In the case of poly-chromatic light, the previous mathematical formalism doesn't hold anymore. In this section will be shown the limitation of the previous formalism, studied the impact of the bandwidth both on the V2MP's condition number and the retrieved mutual coherence function. Experimental results will then be compared to the simulated ones.

2.2.1 Mathematical formalism

Polychromatic V2PM

Using polychromatic light, the interferogram at the n^{th} output can be expressed as a function of the optical path difference, x, as follow :

$$In(x) = \int_{-\infty}^{+\infty} I_A(\sigma)\kappa_A(\sigma)+I_B(\sigma)\kappa_B(\sigma)+2\sqrt{I_A(\sigma)\kappa_A(\sigma)I_B(\sigma)\kappa_B(\sigma)}\,|\mu_{AB}(\sigma)|\,cos(\phi_{AB}(\sigma)+2\pi\sigma x)d\sigma \tag{7}$$

where κ_i relates the transmission from the i^{th} input, I_i the normalized intensity at the i^{th} input, $|\mu_{AB}(\sigma)| = |\mu_{AB}(\sigma)^{inst}| \left|\mu_{AB}(\sigma)^{obj}\right|$ the visibility of the interferogram and $\phi_{AB}(\sigma) = \phi_{AB}^{inst}(\sigma) + \phi_{AB}^{obj}(\sigma)$ the phase of the interferogram. In order to build a V2PM matrix which is independent of the spectrum of the source, it is needed to assume that the spectrum is "flat" within the considered bandwidth. Thus the V2PM matrix will be valid only for quasi-monochromatic light (i.e. a small bandwidth). Doing that the terms I_i are no more wavelength dependant. Eq. **??** becomes :

$$In(x) = t_A \int_\sigma I_A d\sigma + t_B \int_\sigma I_B d\sigma + 2\sqrt{I_A I_B} \int_\sigma \sqrt{\kappa_A(\sigma)\kappa_B(\sigma)}\, |\mu_{AB}(\sigma)|\, cos(\phi_{AB}(\sigma) + 2\pi\sigma x) d\sigma \quad (8)$$

In which $t_i = \frac{\int_\sigma I_i(\sigma)\kappa_i(\sigma)}{\int_\sigma I_i(\sigma)}$. As our assumption lead us to be limited to quasi-monochromatic light, the visibility should also be relatively independent of the wavelength, as well as the phase if the dispersion of the instrument is negligible. Thus Eq.**??** becomes :

$$In(x) = t_A \int_\sigma I_A d\sigma + t_B \int_\sigma I_B d\sigma + 2\sqrt{I_A I_B}\, |\mu_{AB}| \int_\sigma \sqrt{\kappa_A(\sigma)\kappa_B(\sigma)} cos(\phi_{AB} + 2\pi\sigma x) d\sigma \quad (9)$$

From Eq.**??** the measured intensity at the 23 outputs can be linked to the intensity at the 4 inputs by a produce with the V2PM matrix $\{I\} = \{V2PM\}\{V\}$ with :

$$I = \begin{bmatrix} I_1 \\ I_2 \\ \vdots \\ I_{22} \\ I_{23} \end{bmatrix} \qquad V = \begin{bmatrix} \int_\sigma I_A d\sigma \\ \int_\sigma I_B d\sigma \\ \int_\sigma I_C d\sigma \\ \int_\sigma I_B d\sigma \\ \left|\mu_{AB}^{obj}\right| cos(\phi_{AB}^{obj})\sqrt{I_A I_B} \\ \left|\mu_{AB}^{obj}\right| sin(\phi_{AB}^{obj})\sqrt{I_A I_B} \\ \vdots \\ \left|\mu_{CD}^{obj}\right| cos(\phi_{CD}^{obj})\sqrt{I_C I_D} \\ \left|\mu_{CD}^{obj}\right| sin(\phi_{CD}^{obj})\sqrt{I_C I_D} \end{bmatrix},$$

and the V2PM matrix defined by :

$$\begin{bmatrix} t_{A1} & t_{B1} & t_{C1} & t_{D1} & \mathcal{R}\rceil_{AB1} & \mathcal{I}\Updownarrow_{AB1} & \cdots & \mathcal{I}\Updownarrow_{CD1} \\ t_{A2} & t_{B2} & t_{C2} & t_{D2} & \mathcal{R}\rceil_{AB2} & \mathcal{I}\Updownarrow_{AB2} & \cdots & \mathcal{I}\Updownarrow_{CD2} \\ \vdots & \vdots & \vdots & \vdots & \vdots & \vdots & \vdots & \vdots \\ t_{A22} & t_{B22} & t_{C22} & t_{D22} & \mathcal{R}\rceil_{AB22} & \mathcal{I}\Updownarrow_{AB22} & \cdots & \mathcal{I}\Updownarrow_{CD22} \\ t_{A23} & t_{B23} & t_{C23} & t_{D23} & \mathcal{R}\rceil_{AB23} & \mathcal{I}\Updownarrow_{AB23} & \cdots & \mathcal{I}\Updownarrow_{CD23} \end{bmatrix}$$

with $\mathcal{R}\rceil_{ijn} = 2\left|\mu_{ijn}^{inst}\right| \int_\sigma \sqrt{\kappa_{ijn}(\sigma)\kappa_{ijn}(\sigma)} cos(\phi_{ijn}^{inst} + 2\pi\sigma x) d\sigma$, $\mathcal{I}\Updownarrow_{ijn} = -2\left|\mu_{ijn}^{inst}\right| \int_\sigma \sqrt{\kappa_{ijn}(\sigma)\kappa_{ijn}(\sigma)} sin(\phi_{ijn}^{inst} + 2\pi\sigma x) d\sigma$where i, j relates to inputs and n ti the output.

Building the V2PM matrix for a certain x OPD and inverting it by $P2VM = (V2PM^T \times V2PM)^{-1} \times V2PM$, it is possible to retrieve the visibility and phases differences from the 6 baselines by multiplying the P2VM matrix to the I vector independently of the OPD between the inputs.

2.2.2 Influence of the bandwidth

2.2.3 Retrieving the visibility function

3 Laboratory characterization of beam combiners

3.1 Asymmetric couplers

3.2 MMI

3.3 Discrete Beam Combiner

Conclusion and Further-work

A Appendix

A.1 The condition number

Considering the following system $A\vec{x} = \vec{b}$ where A is the matrix describing our system (A is a matrix with real coefficients). An error $\vec{\delta x}$ on $\vec{x}$ will lead to an error $\vec{\delta b}$ on $\vec{b}$. The aim is to know how much bigger or smaller is $\frac{\left\|\vec{\delta x}\right\|}{\|\vec{x}\|}$ compared to $\frac{\left\|\vec{\delta b}\right\|}{\left\|\vec{b}\right\|}$ (i.e how much an error is magnified by the A matrix).

In the case where A in neither symmetric nor square. Then the matrix $A^T A$ is a square symmetric matrix and Then can be diagonalized. Lets call λ_i and $\vec{u_i}$ its eigenvalues and eigenvectors. We can write :

$$A^T A\vec{u_i} = \lambda_i \vec{u_i}$$

Moreover

$$\|A\vec{x}\|^2 = \vec{x}^T A^T A\vec{x} = \left\|\vec{b}\right\|^2$$

So $\left\|\vec{b}\right\|^2 \leq max(|\lambda_i|) \, \|\vec{x}\|^2$ and $\left\|\vec{\delta b}\right\|^2 \geq min(|\lambda_i|) \left\|\vec{\delta x}\right\|^2$ and then :

$$\boxed{\frac{\left\|\vec{\delta x}\right\|}{\|\vec{x}\|} \leq \frac{\sqrt{max(|\lambda_i|)}}{\sqrt{min(|\lambda_i|)}} \frac{\left\|\vec{\delta b}\right\|}{\left\|\vec{b}\right\|}}$$

The number $\frac{\sqrt{max(|\lambda_i|)}}{\sqrt{min(|\lambda_i|)}}$ where $min(|\lambda_i|)$ is the minimal non zero eigenvalue of $A^T A$, is called the condition number of the A matrix. It means how much an error on the right part of the system can be magnified by the A matrix.

Glossary

DBC discrete beam combiner. 1–3

IO Integrated optic. 1

MMI Multi Mode Interferometer. 1

OPD optical path difference. 5, 7

P2VM Pixel to Visibility Matrix. 3

V2PM Visibility to Pixel Matrix. 2, 5, 7

WG waveguide. 5

Bibliography

[BEAS07] Malvin Carl Teich Bahaa E. A. Saleh. *Fundamentals of Photonics.* Wiley Series in Pure and Applied Optics. Wiley-Interscience, 2 edition, 2007.

[DM91] Paul Liao (Eds.) Dietrich Marcuse. *Theory of Dielectric Optical Waveguides.* Academic Press, 2 sub edition, 1991.

[DTL+17] Romina Diener, Jan Tepper, Lucas Labadie, Thomas Pertsch, Stefan Nolte, and Stefano Minardi. Towards 3d-photonic, multi-telescope beam combiners for mid-infrared astrointerferometry. 25:19262, 08 2017.

[Lab08] Pierre Labeye. *Integrated optics components for stellar interferometry.* Theses, Institut National Polytechnique de Grenoble - INPG, February 2008.

[Min12] S. Minardi. Photonic lattices for astronomical interferometry. *Monthly Notices of the Royal Astronomical Society*, 422(3):2656–2660, 2012.

[SMD+13] Allar Saviauk, Stefano Minardi, Felix Dreisow, Stefan Nolte, and Thomas Pertsch. 3d-integrated optics component for astronomical spectro-interferometry. 52:4556–4565, 07 2013.

[TMC+07] Eric Tatulli, F Millour, A Chelli, Gilles Duvert, Bram Acke, Oscar Hernandez Utrera, K H. Hofmann, S Kraus, Fabien Malbet, Mege Pierre, Romain Petrov, Michael Vannier, Gerard Zins, P Antonelli, Udo Beckmann, Y Bresson, Michel Dugue, S Gennari, L Glück, and Noemi Ventura. Interferometric data reduction with amber/vlti. principle, estimators, and illustration. 464, 03 2007.